Supplementary material

Electron cryo-microscopy structure of Ebola nucleoprotein reveals a mechanism for nucleocapsid-like assembly

Zhaoming Su[1,†], Chao Wu[2,†], Liuqing Shi[3,$], Priya Luthra[4,$], Grigore D. Pintilie[5,$], Britney Johnson[2,$], Justin R. Porter[6], Peng Ge[7], Muyuan Chen[5], Gai Liu[2], Thomas E. Frederick[6], Jennifer M. Binning[2], Gregory R. Bowman[6], Z. Hong Zhou[7], Christopher F. Basler[4], Michael L. Gross[3], Daisy W. Leung[2], Wah Chiu[1,*], and Gaya K. Amarasinghe[2,*]

[1]Department of Bioengineering and Department of Microbiology and Immunology, James H. Clark Center, Stanford University, Stanford, CA 94305-5447 USA
[2]Department of Pathology and Immunology, Washington University School of Medicine, St Louis, MO 63110 USA
[3]Department of Chemistry, Washington University in St. Louis, St Louis MO 63130 USA
[4]Center for Microbial Pathogenesis, Institute for Biomedical Sciences, Georgia State University, Atlanta, GA 30303 USA
[5]Verna and Marrs McLean Department of Biochemistry and Molecular Biology, Baylor College of Medicine, Houston, TX 77030 USA
[6]Department of Biochemistry and Molecular Biophysics, Washington University School of Medicine, St Louis, MO 63110 USA
[7]Department of Microbiology, Immunology and Molecular Genetics, University of California, Los Angeles (UCLA), Los Angeles, CA 90095 USA

Supplementary Information included:

Table S1
Figures S1-S6
Movies S1-S3

Movie S1 Segmentations and model docking of three asymmetric units
Movie S2 Probabilistic modeling of eNPs
Movie S3 Illustration of translations and rotations of eNPs

Supplementary Figure Legends

Figure S1. Negative stain electron microscopy of eNP samples in PBS and electrostatic surface potential of eNP-2.

(A) EM images of eNP-2 p1

(B) EM images of eNP-2 p2

(C) EM images of eNP-2 p2 + eVP35 NPBP

(D) Electrostatic surface potential for eNP-2. Red, white, and blue represent negative, neutral, and positive electrostatic potential (-5 to +5 $k_BT\ e^{-1}$). Black box indicates RNA binding groove. Orientation is the same as in Figure 1F.

See also Figure 1.

Figure S2. DLS and HDX-MS characterization of eNP proteins.

(A) DLS data in PBS for: (i) eNP-3 (R_h = 26.3 ± 1.6 nm), and (ii) eNP-3 K373A/K374A/K382A/K383A (R_h = 38.8 ± 3.1 nm). Two independent DLS experiments were performed in triplicate for each construct shown.

(B) Differential HDX-MS highlighted on eNP-2 (PDB: 4YPI); regions not present in the structure are indicated by a dotted line. The color gradient represented differential HDX shown at the bottom is generated by subtracting the amount of deuterium uptake of eNP-3 K373A/K374A/K382A/K383A from that of eNP-3 at the 60 second time point. Regions colored white are not detected by HDX. HDX-MS measurements were performed in duplicate.

See also Figure 2.

Figure S3. Two dimensional classification and Fourier transform of eNP-2 NC-like tubes.

(A) Fourier transform of the raw micrograph with 3.8 Å water ring indicated.

(B) Layer line indexing of eNP-2 tube.

(C) Two-dimensional class averages before applying the rectangular mask, no detailed features observed.

(D) Fourier shell correlation curve before applying mask. Horizontal dashed lines represent the 0.143 FSC cutoff value.

(E) Two-dimensional class averages after applying the rectangular mask, detailed features improved.

(F) Fourier shell correlation curve after applying mask. Horizontal dashed lines represent the 0.143 FSC cutoff value.

(G) Segmented densities for two eNP conformers within an asymmetric unit with rigidly fitted crystal structure 4YPI for molecule a (left) and molecule b (right).

(H) Secondary structure prediction for eNP sequence from residue 361 to 414 using Jpred.

(I) The model after flexible fitting with MDFF to molecule a (left), and the model after creating an extended C-terminal helix α23 and flexible fitting to the density of molecule b (right).

(J) Model to map FSC curves before (green) and after (blue) flexible fitting.

See also Figure 3.

Figure S4. Analysis and characterization of eNP helix α23.

(A) Probabilistic models for eNP-2 molecules 2a and 2b. Orientation is the same as in Figure 3B. The color of the ribbon representation ranges from green to orange to indicate

variance in atomic positions at each residue (green, σ = 0.2 Å; red, σ = 2.7 Å). A majority of the ribbon are colored dark to light green indicating low variance. Other parts with higher variance and uncertainty include loop regions, such as that highlighted in the boxed region.

(B) FP assay of unlabeled eVP35 NPBP peptide (black) or eNP 370-411 peptide (red) competing against FITC-eVP35 NPBP binding to eNP-2. Each measurement was performed two times independently in duplicate.

(C) ITC experiment showing no heat from binding of eNP 370-411 peptide to eNP-2. Each measurement was performed in duplicate.

(D) Electrostatic surface potential for eNP shows eNP oligomerization interfaces have alternating complementary charge distribution. Red, white, and blue represent negative, neutral, and positive electrostatic potential (-5 to +5 $k_BT\ e^{-1}$). RNA binding grooves locates within the hinge region between N- and C-lobe.

See also Figure 3.

Figure S5. eNP conformational heterogeneity and proposed mechanism for eNP oligomerization and RNA binding.

(A) eNP samples oligomer-like conformations even in the monomeric state. Overlay of a structural state from our MSM (blue) with the holo crystal structure (eNP in green, eVP35 NPBP in magenta) and a monomer from the cryoEM structure (gray).

(B) A proposed mechanism showing that eNP oligomerization is required for RNA binding.

See also Figure 5.

Figure S6. A comparison of the eNP assembly from this study with the eNP assemblies from Wan et al.

(A) Side views of the eNP 1-450 assembly (left) and the eNP-eVP24-eVP35-eVP40 VLP structure (middle) by Wan et al. and the eNP assembly from this study (right). eVP24 subunits from the VLP structure are colored in magenta and yellow (middle). Two eNP-2 molecules in the asymmetric unit from the current study are highlighted in cyan and blue (right).

(B) Six representative eNP molecules from the corresponding assemblies shown in (A) (top). View of the middle two eNP molecules rotated 90º (bottom). The RNA contact surfaces on eNP from the VLP structure are colored in orange and the eVP24 contact surfaces on eNP from the VLP structure are colored in magenta and yellow (middle). This coloring is imposed on the eNP 1-450 assembly (left) and the structure from this study (right). Mapping of the eNP contact surfaces for RNA and eVP24 binding to the eNP-2 assembly from this study suggests potential steric clashes and that the two assemblies are distinct. The red dotted circle on the right panel structure highlights that one set of modeled eVP24 contact interfaces from VLP structure (middle) are not accessible in the structure from the present study.

Table S1. Statistics for cryoEM map.

See also Figure 3.

Figure S1, related to Figure 1

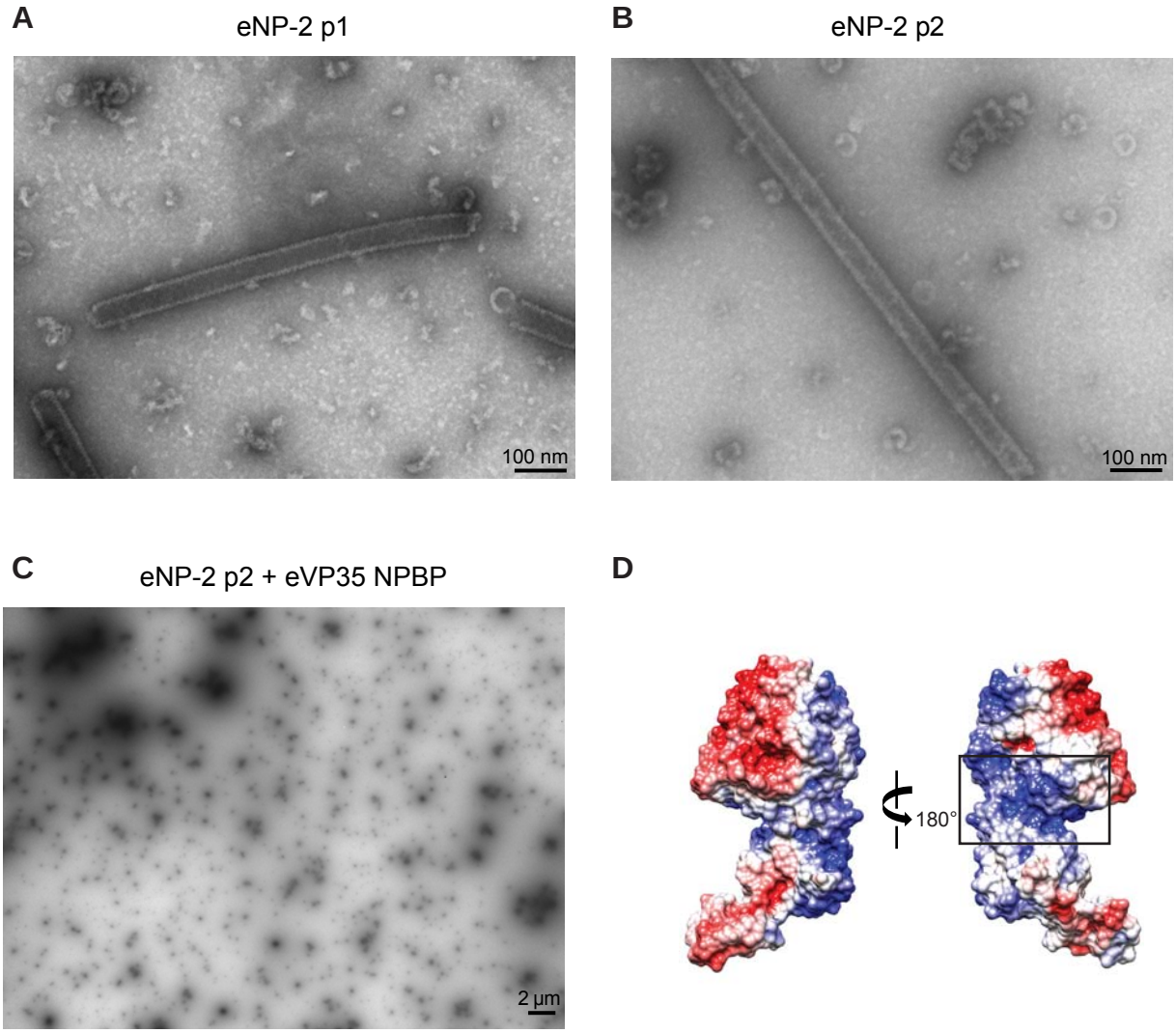

Figure S2, related to Figure 2

A

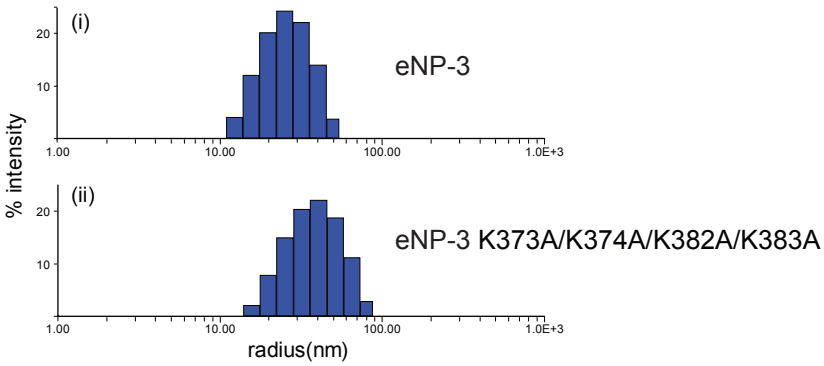

B

eNP-3 vs eNP-3 K373A/K374A/K382A/K383A

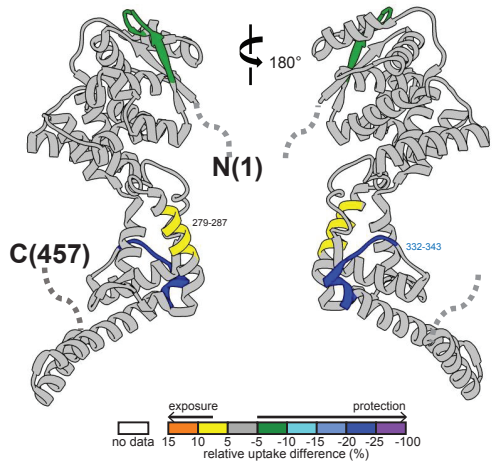

Figure S3, related to Figure 3

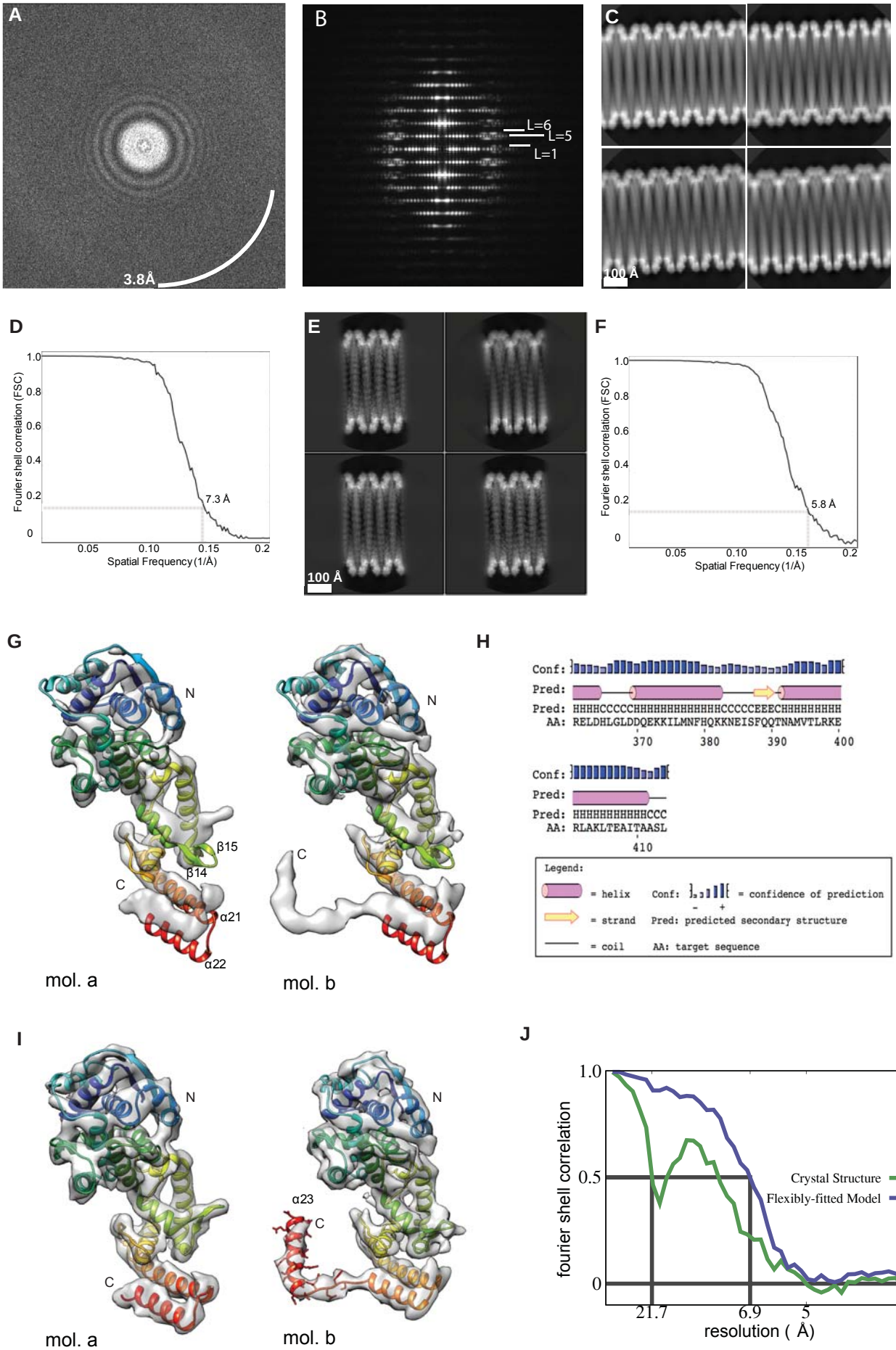

Figure S4, related to Figure 3

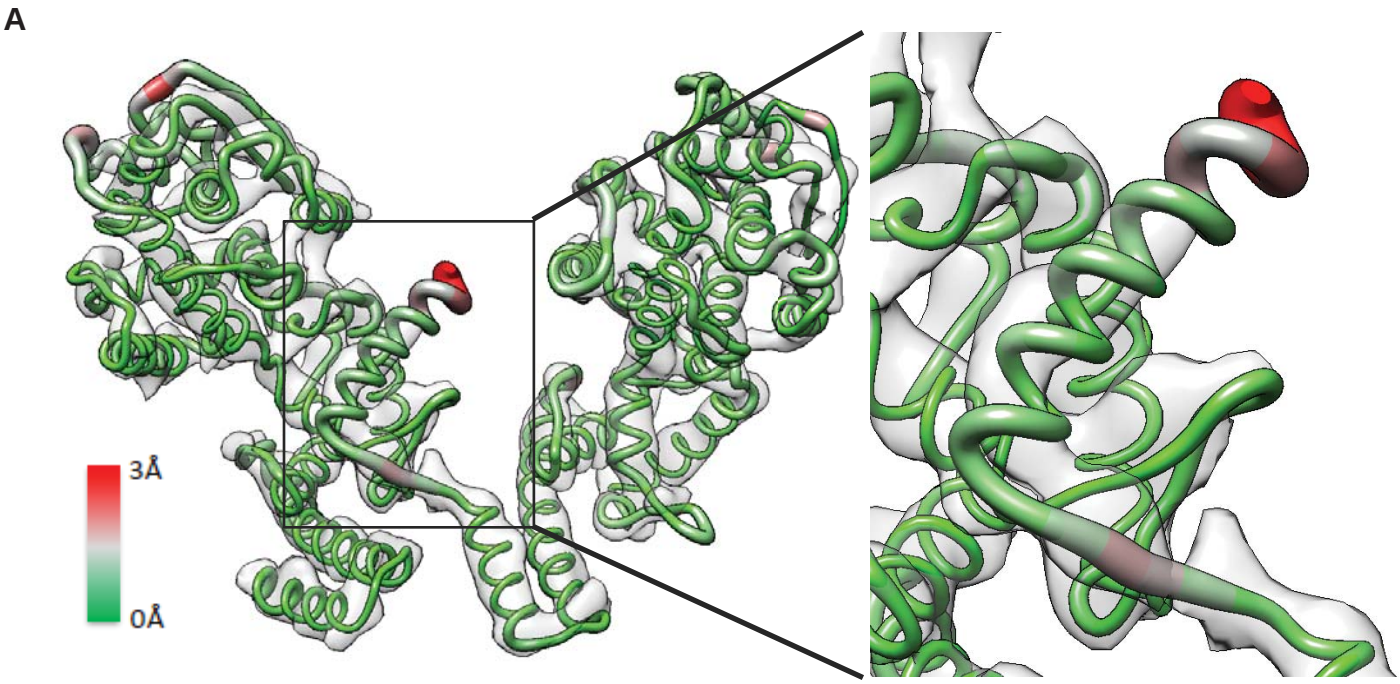

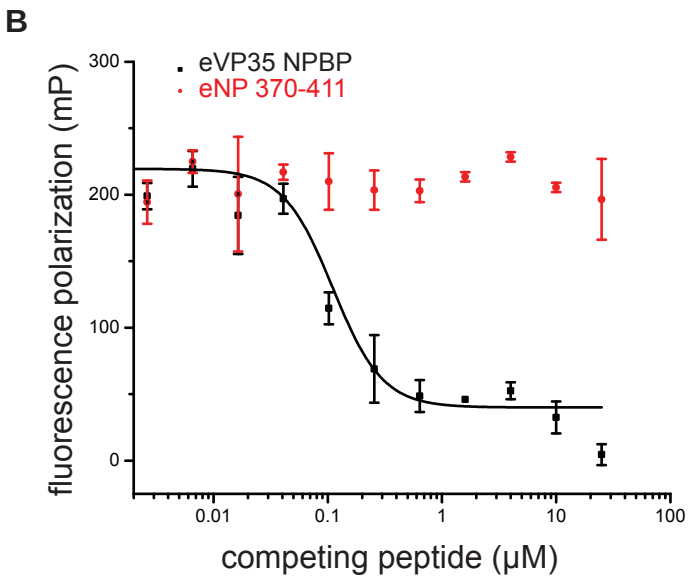

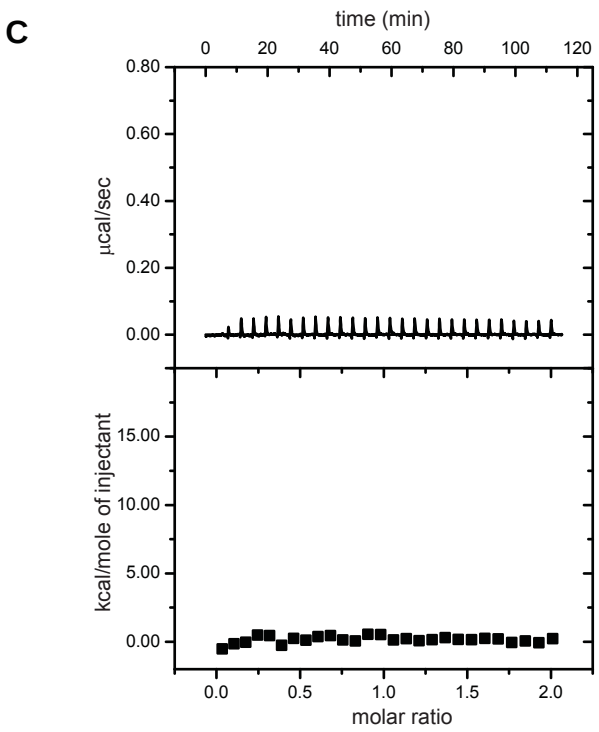

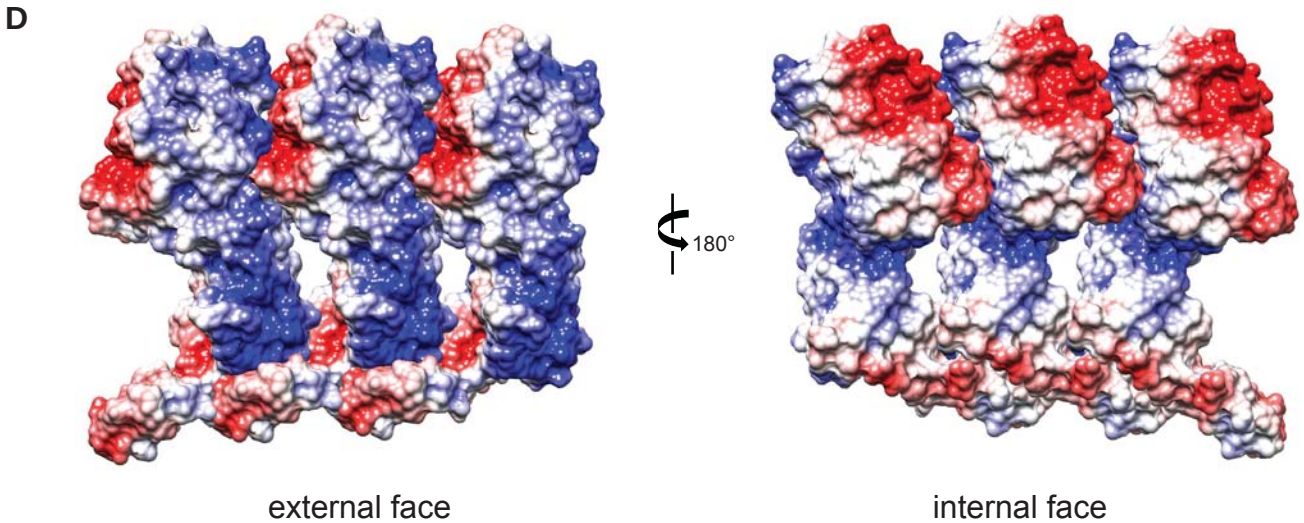

Figure S5, related to Figure 5

A

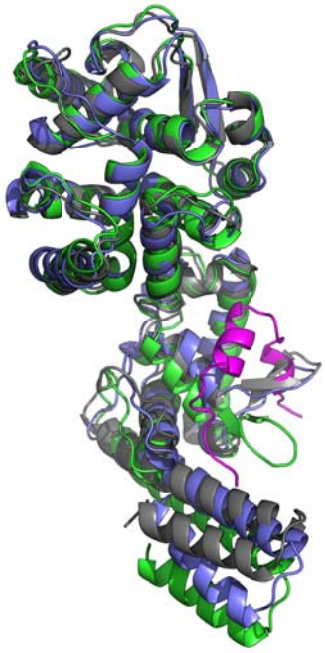

B

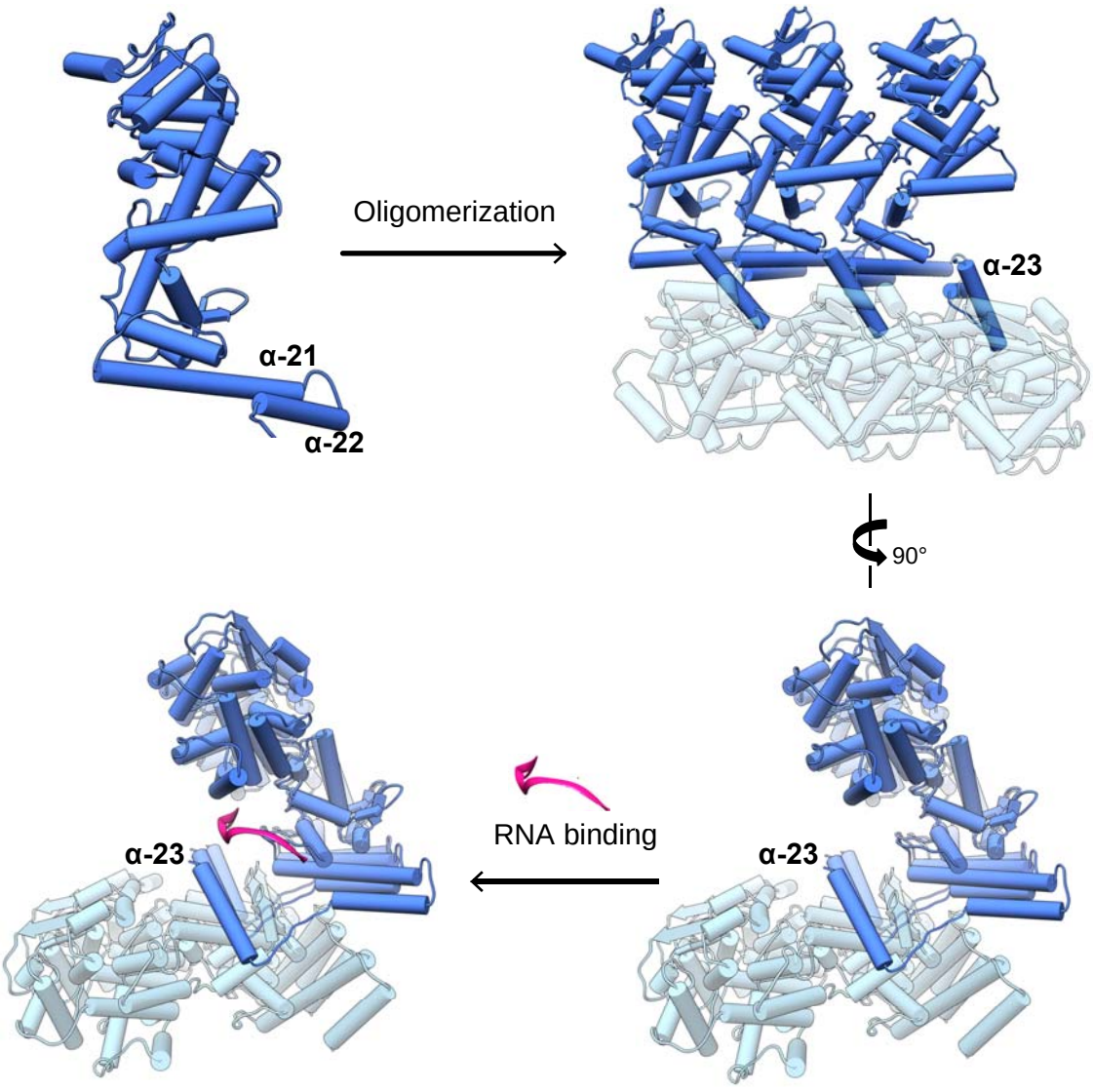

Figure S6, related to Figure 5

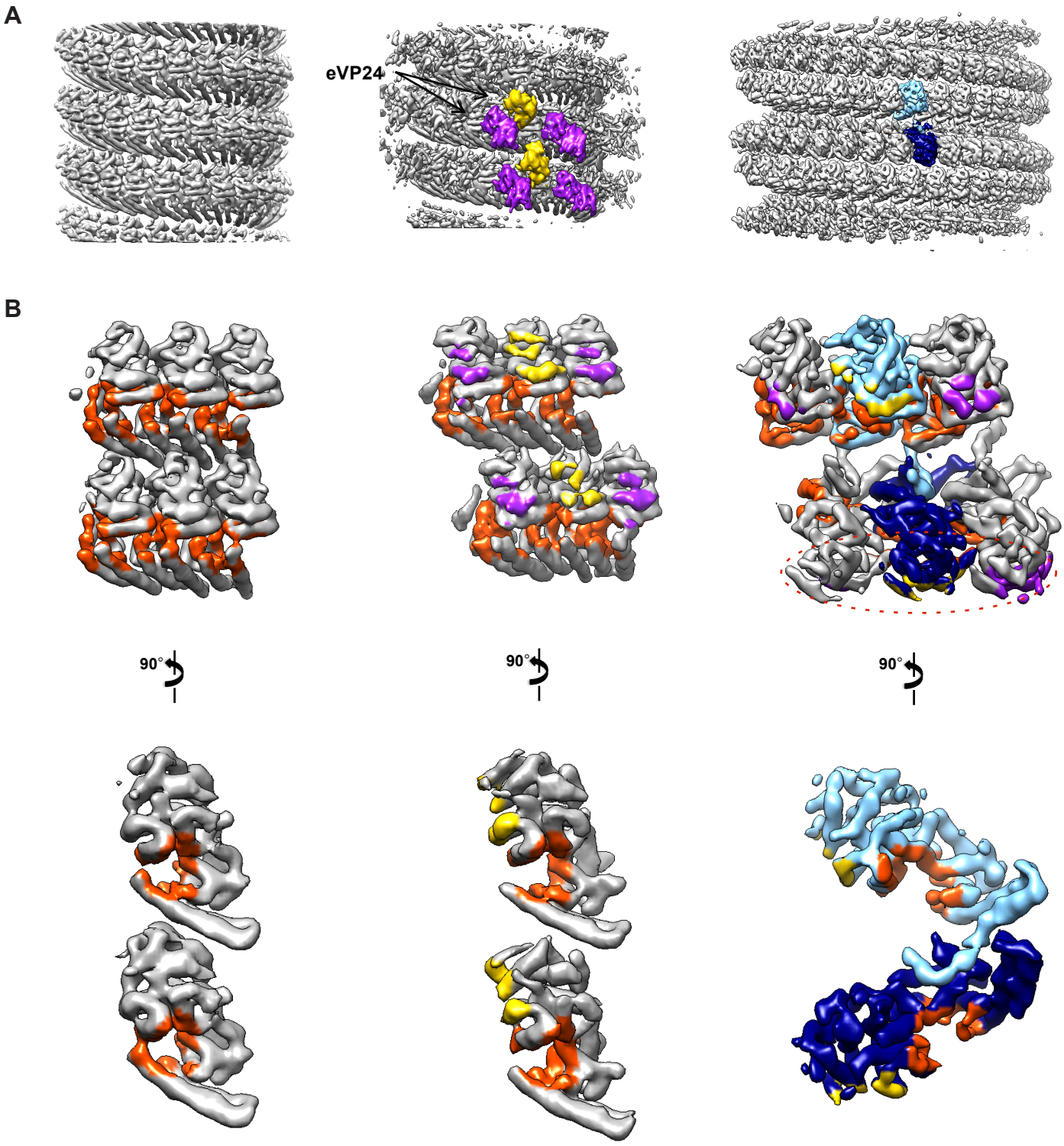

Table S1. Electron cryomicroscopy data collection and processing of eNP-2 structure

Microscope	JEM3200FSC
Voltage (kV)	300
Energy filter slit width (eV)	30
Detector	Gatan K2 Summit
Magnification	30,000X
Pixel size (Å)	1.2
Defocus range (μm)	0.5 – 2.0
Electron exposure ($e^-/Å^2$)	24
Micrographs (acquired/used)	1266 / 1113
Segment step (asymmetric unit)	5
Number of segments/asymmetric unit	169,526 / 847,630
Helical twist and rise (°/Å)	-8.53 / 2.65
Map resolution at 0.143 FSC criterion (Å)	5.8